Full length article

Ultramafic to mafic granulites from the Larsemann Hills, East Antarctica: Geochemistry and tectonic implications

Laixi Tong[a,*], Bor-ming Jahn[b], Xiaohan Liu[c], Xirong Liang[a], Yi-gang Xu[a], Dmitri Ionov[a,d]

[a] State Key Lab of Isotope Geochemistry, Guangzhou Institute of Geochemistry, Chinese Academy of Sciences, Guangzhou 510640, China
[b] Department of Geosciences, National Taiwan University, Taipei 106, Taiwan
[c] Institute of Tibetan Plateau, Chinese Academy of Sciences, Beijing 100085, China
[d] Geosciences Montpellier, Montpellier University, Montpellier 34095, France

ARTICLE INFO

ABSTRACT

The Larsemann Hills area is part of a reworked early Neoproterozoic metamorphic terrain in southwestern Prydz Bay, East Antarctica. Ultramafic and mafic granulites, whose origins remain controversial, occur as lenses, boudins or layered bodies within the para- and ortho-gneiss in the region. The ultramafic and mafic granulites show spinel-olivine-bearing and two-pyroxene-bearing mineral assemblages recrystallized at 860–900 °C. Their bulk rock analyses indicate an origin as igneous cumulates, with high $Mg^{\#}$ (molar $MgO/(MgO + FeO)$) from 0.73 to 0.84 for ultramafic granulite and from 0.46 to 0.78 for mostly mafic granulite as well as high Cr and Ni contents ([Cr] and [Ni] up to 1826 ppm and 1400 ppm respectively for ultramafic granulite and [Cr] of 1460 ppm for mafic granulite). Trace element patterns show pronounced negative Nb anomalies, suggesting a subduction-related tectonic setting for their precursors, consistent with derivation from arc basalts, also suggested by low TiO_2 and K-enrichment in mafic granulites. The ultramafic to mafic granulites may have been formed in a subduction-related continental back-arc basin environment simultaneously with peak metamorphism associated with arc-continent collision during the early Neoproterozoic (990–900 Ma) Rayner orogeny.

1. Introduction

The Prydz Bay region in East Antarctica comprises three major geological units from east to west (Fig. 1): (1) the Vestfold Hills, a late Archean craton block stabilised at 2500 Ma (Black et al., 1991), with abundant Proterozoic mafic dyke swarms (Lanyon et al., 1993) overprinted by early Neoproterozoic granulite facies metamorphism (Liu et al., 2014); (2) the Rauer Group, a reworked composite Archean-Proterozoic gneiss terrain (Harley et al., 1995; Kinny et al., 1993) overprinted by an early Palaeozoic (~530 Ma) thermal event (Dirks and Wilson, 1995; Harley et al., 1995) and affected by the development of sapphirine-bearing ultrahigh-temperature metapelitic granulites (Harley, 1998; Tong and Wilson, 2006); (3) the southwestern Prydz Bay region, including the Larsemann Hills and adjacent areas, which represents a reworked early Neoproterozoic metamorphic terrain dominated by the paragneiss and mafic-felsic composite orthogneiss and also affected by the Pan-African thermal event (~530 Ma) (Tong et al., 1998, 2002; Wang et al., 2008; Grew et al., 2012). In the last two decades, the southwestern Prydz Bay region has been recognised as an important part of the early Palaeozoic Pan-African (550–500 Ma)

tectonic mobile belt (the Prydz Belt) in East Antarctica (Carson et al., 1996; Dirks and Wilson, 1995; Fitzsimons et al., 1997; Hensen and Zhou, 1995; Zhao et al., 1995). Furthermore, it was considered as a Pan-African suture zone associated with the final assembly of East Gondwana supercontinent (Fitzsimons et al., 1997; Hensen and Zhou, 1997; Fitzsimons, 2003; Zhao et al., 2003). However, more recently, new geochronological and metamorphic data support the scenario whereby the high-grade metamorphic rocks in the Prydz Belt (including the Larsemann Hills and areas towards the eastern Amery Ice Shelf) actually represent part of a reworked early Neoproterozoic Rayner Complex (Wilson et al., 2007; Wang et al., 2008; Liu et al., 2009; Grew et al., 2012; Tong et al., 2014).

According to this recent reassessment, the Larsemann Hills and adjacent areas were also affected by the early Palaeozoic Pan-African tectono-thermal event (Wang et al., 2008; Grew et al., 2012; Liu et al., 2013; Tong et al., 2014). Ultramafic to mafic granulites in the region occur as lenses, pods or layered bodies in paragneisses and felsic orthogneisses. Their origins have been controversial until recently. Some workers considered the ultramafic to mafic granulites to represent the remnants of mafic dykes or sills tectonized in the early Neoproterozoic
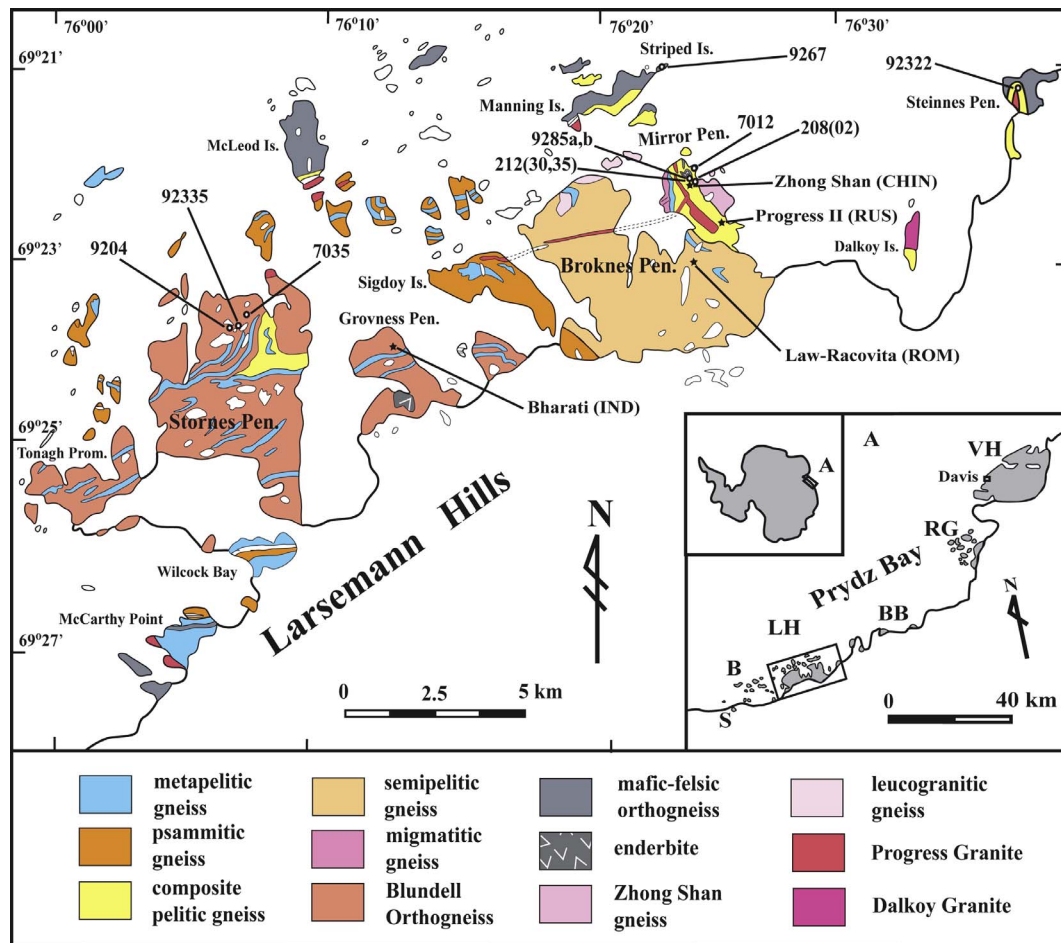
Fig. 1. Geological map of the Larsemann Hills, Prydz Bay, East Antarctica, showing major lithological units and sample locations (modified after Tong et al., 2014). Insert shows the position of the Larsemann Hills in Prydz Bay. Abbreviations: LH, Larsemann Hills, S, Søstrene Island, B, Bolingen Islands, BB, Brattstrand Bluffs, RG, Rauer Group, VH, Vestfold Hills.

(Thost et al., 1992) or in the early Palaeozoic (Wang et al., 1994). Others, by contrast, believed that they formed in a collision-related subduction zone in the early Palaeozoic Pan-African event (Ren et al., 1992) because their modes of occurrence are similar to those of similar rocks in the Lützow-Holm Complex (Hiroi et al., 1991). Recently, new geochemical data provided evidence that the ultramafic to mafic granulites in the region likely formed in an arc-related subduction zone setting, or in a continental collision-related environment during the late Mesoproterozoic or early Neoproterozoic orogeny (Tong et al., 2006; Liu et al., 2014).

Here, we have undertaken detailed petrological and geochemical studies in order to constrain the origin of the ultramafic to mafic granulites in the Laremann Hills because these rocks contain important information on tectonic evolution history of the early Neoproterozoic Rayner complex in the Prydz Belt. The results of the study, combined with data on other granulite assemblages, their metamorphic P-T trajectories and regional chronological data in the region, support the suggestion that these rocks may have been formed simultaneously with related peak metamorphism in a subduction-related continental back-arc basin associated with arc-continent collision during the early Neoproterozoic (990–900 Ma) Rayner orogeny.

2. Geological background

The Larsemann Hills, located in the central part of the southwestern Prydz Bay coast, are composed mainly of upper amphibolite to granulite facies psammitic to pelitic paragneiss, mafic-felsic composite orthogneiss and the Blundell Orthogneiss (970–980 Ma), with minor leucogranitic gneiss, mafic to ultramafic granulite, syn- or post-tectonic

granite and late pegmatite (Fig. 1) (Carson et al., 1995a; Carson and Grew, 2007; Grew et al., 2012). The paragneiss and composite orthogneiss sequences were also referred to as the Brattstrand Paragneiss and Søstrene Orthogneiss respectively by Fitzsimons (1997) for the metasedimentary and mafic-felsic metaigneous units in the region and adjacent areas along the southwestern Prydz Bay coast (Stüwe et al., 1989; Thost et al., 1991; Carson et al., 1995a; Fitzsimons, 1997; Grew et al., 2012). Some paragneisses contain borosilicate minerals prismatine and grandidierite (Ren et al., 1992; Carson et al., 1995b; Grew et al., 2006, 2013; MacGregor et al., 2013); sapphirine-bearing assemblages were also reported from Stornes Peninsula in the same area (Fig. 1) (Tong et al., 1997; Tong and Liu, 1997; Grew et al., 2006, 2007; Ren et al., 2008). The paragneisses experienced extensive partial melting and migmatization (Dirks et al., 1993), and were considered to represent part of an extensive sedimentary basin sequence extending about 130 km from the southern Rauer Group to the Bolingen Islands (Carson et al., 1995a). The mafic-felsic orthogneisses and paragneisses in the region were generally interpreted as a tectonically interleaved Proterozoic basement and sedimentary cover sequence (Sheraton et al., 1984; Stüwe et al., 1989; Fitzsimons and Harley, 1991; Dirks et al., 1993; Carson et al., 1995a; Dirks and Hand, 1995).

The Larsemann Hills region was initially considered to have undergone a major low-pressure granulite facies metamorphism in the late Mesoproterozoic (~1100 Ma), with peak conditions of 4.5 kbar and 750 °C (Stüwe and Powell, 1989). However, later it was alternatively suggested that this low-pressure granulite facies metamorphism occurred in the early Palaeozoic (550–500 Ma) as a result of a Pan-African collisional tectonism, but that the complex also preserved relics of an earlier metamorphic event with conditions of 9 kbar and 850 °C (Ren

et al., 1992). Furthermore, other researchers argued that the region and adjacent areas experienced a single Pan-African metamorphism related to collisional tectonism, with higher peak P-T conditions of 6–7 kbar and 800–860 °C (Fitzsimons, 1996; Carson et al., 1997; Grew et al., 2006). This was mainly based on the assumption that the paragneiss precursor was deposited during the Neoproterozoic, and was not affected by the ∼1000 Ma metamorphic event (Hensen and Zhou, 1995; Zhao et al., 1995; Fitzsimons, 1997). Nevertheless, some early (∼1000 Ma) structural-metamorphic relics (including the paragneiss) with higher P-T conditions of 9–10 kbar and 870–980 °C were reported from the same region and adjacent areas (Dirks and Hand, 1995; Tong and Liu, 1997), while those close to peak P-T conditions (∼10 kbar and ∼1000 °C) were reported from the Søstrene Island (Thost et al., 1991; Hensen and Zhou, 1995). Moreover, more recently obtained isotopic data support the suggestion that this region and adjacent areas indeed experienced two major metamorphic events, an early one at ∼1000 Ma, and a later one at ∼530 Ma (Zhang et al., 1996; Tong et al., 1998, 2002; Wang et al., 2008; Grew et al., 2012), which are consistent with a recent study of metamorphic P-T history of the region (Tong et al., 2014).

Structural studies showed that the study region was affected by at least four phases of deformation (Dirks et al., 1993; Carson et al., 1995a; Dirks and Hand, 1995). As suggested by recent SHRIMP U-Pb zircon ages (Wang et al., 2008; Grew et al., 2012), D1 high-grade deformation associated with interleaving of felsic and sedimentary rocks and granulite facies metamorphism (M1) occurred at ∼1000 Ma, followed by intrusion of felsic and mafic intrusives at 970–980 Ma. The early D1 deformation mainly occurs as intrafolial F1 folding (Stüwe et al., 1989; Carson et al., 1995a). D2 deformation related to SE to NW high-grade transpression formed regional gneissic foliation S2, accompanied by granulite facies metamorphism (M2) at ∼530 Ma. These events were followed by D3 high-strain extensional deformation, and intrusion of granites and regional NW-trending pegmatites in the study region and other adjacent areas in Prydz Bay (Carson et al., 1995a; Dirks and Hand, 1995; Dirks and Wilson, 1995). D4 deformation is confined to discrete dextral, normal mylonite zones with amphibolite facies metamorphism along the margins of NW-trending planar pegmatites in the region (Carson et al., 1995a).

3. Field relations and modes of occurrence

Ultramafic to mafic granulites were reported sporadically from the southwestern Prydz Bay region (Stüwe et al., 1989; Thost et al., 1991, 1992; Fitzsimons and Harley, 1991). In the Larsemann Hills, ultramafic granulites comprise less 1% of outcrops on Stornes Peninsula, Striped Island, Mirror Peninsula and Steinnes Peninsula (Fig. 1) (Stüwe et al., 1989), and were also reported from adjacent areas (e.g. Bolingen Islands and Brattstrand Bluffs) (Fig. 1) (Fitzsimons and Harley, 1991; Thost et al., 1992). They generally occur as small pods, lenses and narrow layers (Manning Island), oriented parallel to the gneissic foliation, both in paragneiss and orthogneiss (Wang et al., 1994; Tong et al., 2006). Mafic granulites normally occur in the region as large boudins or layered bodies in the composite mafic-felsic orthogneiss.

The ultramafic granulite pods or lenses are generally 0.5–1.5 m in size, and may be as small as 5–10 cm (Fig. 2). The mafic granulite boudins or layered bodies are usually 0.5–2.0 m in width and 1–10 m in length. According to their modes of occurrence in the field and mineral assemblages (Table 1), these ultramafic to mafic granulites can be divided into three types as follows: (1) dark spinel-olivine-two-pyroxene-bearing ultramafic granulites, likely derived from lherzolites, mainly present in the northern Stornes Peninsula, representative samples are 9204, 92335 and 7035; (2) greenish two-pyroxene-bearing ultramafic granulites, probably metamorphosed from pyroxenites, found on Striped Island and Steinnes Peninsula, typical samples are 9267 and 92322; and (3) dark two-pyroxene-plagioclase-bearing mafic granulites, representative samples 9285a, 9285b and 7012, mainly from the

northern Mirror Peninsula (Fig. 1) (Table 1). Three mafic granulite samples reported by Wang et al. (1994) from the northern Mirror Peninsula are also shown in Fig. 2.

4. Analytical methods

Chemical compositions of minerals were determined by electron probe micro-analysis (EPMA) in thin sections on a Cameca Camebax-Microbeam SX-51 at the Institute of Geology and Geophysics, Chinese Academy of Sciences, Beijing. The operating conditions were 25 nA beam current and a 5 μm beam, with an accelerating voltage of 15 kV. Data were reduced with the Cameca PAP matrix correction program (Pouchou and Pichoir, 1984). Fe^{3+} contents were estimated by charge balance calculations. Representative analyses of mineral compositions in typical assemblages are given in Table 2.

The rock samples were crushed and ground in an agate ring mill. Major elements in the whole-rock (WR) powders were determined by X-ray fluorescence (XRF) spectrometry, while trace elements were measured with a PE Elan 6000 inductively coupled-plasma mass spectrometer (ICP-MS) at the Guangzhou Institute of Geochemistry, Chinese Academy of Sciences, Guangzhou. Analytical uncertainties are mostly ± 1–3% for major elements, and ± 5% for most trace elements. The analytical procedures followed those described by Li et al. (2006).

5. Petrography and recrystallization conditions

5.1. Petrography

As noted above, the ultramafic to mafic granulites can be divided into three types. Representative microphotos illustrating their mineral assemblages and textural relations are shown in Fig. 3. Those for mafic granulites are not provided here, because they have been already reported by Ren et al. (1992), Wang et al. (1994) and Tong et al. (1995). Their detailed descriptions are as follows.

(1) *Dark ultramafic granulites* are mainly composed of spinel (Spl), olivine (Ol), orthopyroxene (Opx), clinopyroxene (Cpx), amphibole (Amp), and minor biotite (Bt), magnesite (Mag), dolomite (Dol) and opaque minerals such as magnetite (Mt) (Table 1). Olivine grains are strongly deformed; orthopyroxene encloses spinel in sample 9204 (Fig. 3a), secondary magnesite surrounding a clinopyroxene and dolomite surrounding a spinel are also observed (Fig. 3b). In addition, a spinel-amphibole-biotite assemblage occurs as inclusions in olivine in sample 92335, and spinel grains also occur interstitially or as inclusions (Fig. 3c). No decompression textures are observed in thin sections.

(2) *Greenish ultramafic granulites* consist mainly of orthopyroxene, clinopyroxene, and minor amphibole, biotite, plagioclase (Pl) and quartz (Qz) (Table 1). For sample 9267, an orthopyroxene grain is entirely enclosed in relatively coarse clinopyroxene (Fig. 3d). Sample 92322 contains less biotite than sample 9267 (Fig. 3e), small orthopyroxene and clinopyroxene grains as well as quartz occur as inclusions in large clinopyroxene grains (Fig. 3f). Likewise, no apparent decompression textures are observed.

(3) *Dark mafic granulites* show massive textures with weak foliation; they are mainly composed of coarse orthopyroxene, clinopyroxene, amphibole, biotite, plagioclase, and minor quartz and magnetite (Table 1). Their mineral assemblages and textures were described in detail by Ren et al. (1992). In this study, samples 9285a and 9285b are from different layers in an outcrop of mafic granulite, the latter containing more biotite and less plagioclase. Sample 7012 contains more quartz and much less amphibole than samples 9285a and 9285b.
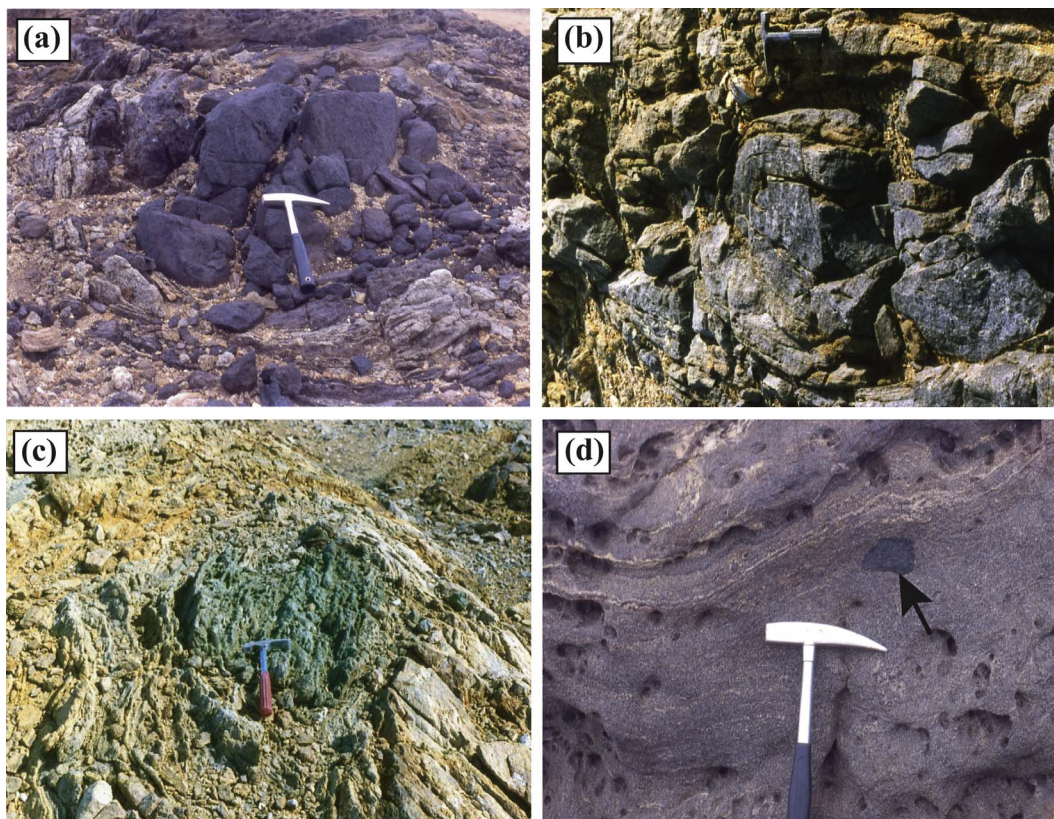
Fig. 2. The field photographs showing the modes of occurrence of the ultramafic granulites from the Larsemann Hills: (a) dark ultramafic granulite sample 9204 in the host paragneiss from Stornes Peninsula; (b) deformed ultramafic granulite sample 92335 hosted by paragneiss from Stornes Peninsula; (c) greenish ultramafic granulite sample 92322 in the host felsic orthogneiss from Steiness Peninsula; (d) small dark ultramafic granulite hosted by mafic orthogneiss from Stornes Peninsula. The hammer used as a scale is 30 cm long.

5.2. Mineral chemistry

This study focuses on the compositions of typical minerals in the ultramafic granulites because those for mafic granulites in this region have been reported by Ren et al. (1992). EPMA data for representative minerals of the ultramafic granulites are given in Table 2.

Spinel has X_{Mg} values [= molar $Mg/(Mg + Fe^{2+})$] of 0.43–0.61 and relatively high Cr_2O_3 (up to 7.09 wt%) (Table 2), which is lower than 11.25 wt% for spinel reported from an ultramafic granulite in Bolingen Islands by Thost et al. (1992).

Olivine is relatively magnesian, with X_{Mg} of 0.78 in sample 92335 and 0.69 in sample 9204, respectively (Table 2).

Orthopyroxene in the dark ultramafic granulite has higher Al_2O_3 than that in greenish ultramafic granulite at similar X_{Mg} (Table 2). For instance, in samples 9204 and 92322, the orthopyroxene has 3.13–3.75 wt% Al_2O_3, higher than 0.87–1.06 wt% in samples 9267 and 92322 (Table 2), but all the orthopyroxenes show similar X_{Mg} ranging

from 0.77 to 0.82.

Clinopyroxene in the dark ultramafic granulite likewise has higher Al_2O_3 than that of the clinopyroxene in greenish ultramafic granulite. For example, the clinopyroxene in sample 9204 has 4.01 wt% Al_2O_3, higher than 0.91–1.49 wt% in the clinopyroxene in samples 9267 and 92322 (Table 2), whilst they show similar X_{Mg} of 0.87 and 0.82–0.91.

Composition of the amphibole corresponds to pargasite. The amphibole in dark ultramafic granulite has lower X_{Mg} than amphibole in greenish ultramafic granulite. For instance, the X_{Mg} of amphibole in samples 9204 and 92335 are 0.73–0.78, i.e. lower than that (0.91) in sample 92322 (Table 2).

Biotite is relatively magnesian as well, and its composition corresponds to phlogopite. For example, biotites in samples 92335 and 9267 have MgO contents of 19.99 wt% and 23.02 wt%, respectively, and the X_{Mg} values of 0.82 and 0.88 (Table 2).

Plagioclase is anorthite-rich, and their compositions of plagioclase in samples 9267 and 92322 are $An_{76}Ab_{24}Or_{00}$ and $An_{82}Ab_{18}Or_{00}$,

Table 1
Mineral assemblages in the ultramafic and mafic granulites from the Larsemann Hills. Abbreviations: Spl, spinel, Ol, olivine, Opx, orthopyroxene, Cpx, clinopyroxene, Amp, amphibole, Bt, biotite, Hb, hornblende, Pl, plagioclase, Qtz, quartz, Mt, magnetite, Dol, dolomite, Mag, magnesite.

Rock type	Sample	Location	Primary minerals									Secondary minerals				Field occurrence
			Spl	Ol	Opx	Cpx	Amp	Bt	Pl	Qz	Mt	Hb	Bt	Dol	Mag	
Ultramafic granulite	9204	Stornes Pen.	x	x	x	x	x				x			x	x	Dark pod or lens
	92335	Stornes Pen.	x	x	x		x	x			x					Dark pod or lens
	7035	Stornes Pen.	x	x	x	x	x									Dark pod or lens
	9267	Striped Island			x	x		x	x	x						Green pod or lens
	92322	Steinnes Pen.			x	x	x		x	x						Green pod or lens
Mafic granulite	9285a	Mirror Pen.			x	x	x		x	x			x			Dark boudin
	9285b	Mirror Pen.			x	x	x		x	x			x			Dark boudin
	7012	Mirror Pen.			x	x			x	x	x	x				Dark boudin

Table 2

Representative chemical analyses of minerals (weight% and formula units) in the ultramafic granulite samples from the Larsemann Hills. For mineral abbreviations see Table 1.

	9204					92335					9267				92322			
	Ol	Spl	Opx	Cpx	Amp	Ol	Spl	Opx	Amp	Bt	Opx	Cpx	Bt	Pl	Opx	Cpx	Amp	Pl
SiO_2	39.01	0.22	52.93	50.64	42.80	37.49	0.04	52.67	42.11	37.40	54.05	53.13	41.50	49.39	54.94	53.95	48.68	47.87
TiO_2	0.00	0.00	0.12	0.78	1.74	0.00	0.16	0.10	2.18	2.87	0.00	0.06	1.89	0.05	0.05	0.08	0.28	0.01
Al_2O_3	0.06	62.02	3.13	4.05	13.68	0.22	50.35	3.75	14.77	16.09	0.87	0.91	12.90	31.06	1.06	1.49	8.52	32.20
Cr_2O_3	0.00	1.94	0.05	0.08	0.12	0.00	7.09	0.06	0.39	0.64	0.10	0.25	0.48	0.02	0.32	0.66	1.17	0.00
Fe_2O_3	0.00	0.00	2.51	1.36	0.00	0.00	7.32	0.00	0.00	0.00	1.59	0.00	0.00	0.00	1.39	0.83	0.00	0.00
MgO	40.76	16.62	28.36	14.61	15.63	34.44	9.98	26.35	14.06	19.99	27.28	16.50	23.02	0.02	29.72	16.56	20.01	0.01
CaO	0.01	0.00	0.54	23.92	12.81	0.00	0.05	0.36	11.95	0.00	0.70	22.19	0.00	15.91	0.44	23.68	12.85	16.97
MnO	0.28	0.07	0.28	0.08	0.10	0.38	0.24	0.23	0.16	0.02	0.24	0.21	0.05	0.00	0.29	0.18	0.11	0.00
FeO	20.20	19.52	11.57	3.89	7.97	27.27	23.90	16.6	9.22	8.11	14.89	5.65	5.40	0.00	11.79	2.81	3.50	0.01
NiO	0.22	0.00	0.12	0.03	0.05	0.00	0.17	0.00	0.00	0.17	0.00	0.04	0.17	0.00	0.06	0.04	0.02	0.00
Na2O	0.01	0.00	0.04	0.10	2.27	0.00	0.03	0.26	1.98	0.49	0.00	0.20	0.32	2.77	0.01	0.33	1.48	2.06
K_2O	0.00	0.01	0.01	0.02	0.68	0.00	0.02	0.00	1.44	9.23	0.00	0.00	10.09	0.08	0.00	0.05	1.55	0.09
Total	100.50	100.40	99.64	99.59	97.83	99.79	99.34	100.38	98.29	95.12	99.72	99.12	95.88	99.30	100.08	100.66	98.25	99.22
O	4	4	6	6	24	4	4	6	24	22	6	6	22	8	6	6	24	8
Si	1.000	0.006	1.898	1.874	6.192	1.001	0.001	1.890	6.104	5.435	1.985	1.971	5.891	2.276	1.954	1.958	6.856	2.213
Ti	0.000	0.000	0.003	0.022	0.189	0.000	0.003	0.003	0.238	0.313	0.000	0.002	0.202	0.002	0.001	0.002	0.031	0.000
Al	0.000	1.902	0.132	0.177	2.332	0.007	1.681	0.159	2.525	2.754	0.037	0.040	2.159	1.687	0.044	0.064	1.413	1.756
Cr	0.000	0.040	0.001	0.002	0.014	0.000	0.159	0.002	0.045	0.074	0.003	0.007	0.055	0.001	0.009	0.019	0.131	0.000
Fe^{3+}	0.000	0.000	0.068	0.038	0.000	0.000	0.156	0.072	0.000	0.000	0.041	0.000	0.000	0.000	0.037	0.023	0.000	0.000
Mg	1.557	0.650	1.516	0.806	3.370	1.371	0.421	1.410	3.041	4.330	1.473	0.918	4.870	0.001	1.576	0.896	4.201	0.001
Ca	0.000	0.000	0.021	0.948	1.986	0.000	0.001	0.014	1.857	0.000	0.027	0.882	0.000	0.785	0.017	0.921	1.939	0.841
Mn	0.006	0.002	0.009	0.003	0.011	0.009	0.006	0.007	0.020	0.002	0.007	0.007	0.006	0.000	0.009	0.006	0.013	0.000
Fe^{2+}	0.433	0.424	0.347	0.120	0.964	0.609	0.566	0.427	1.119	0.985	0.451	0.175	0.642	0.000	0.351	0.085	0.412	0.000
Ni	0.005	0.005	0.003	0.001	0.006	0.000	0.004	0.000	0.000	0.020	0.000	0.001	0.019	0.000	0.002	0.001	0.002	0.000
Na	0.001	0.000	0.003	0.008	0.638	0.000	0.001	0.018	0.568	0.138	0.000	0.001	0.088	0.247	0.001	0.024	0.405	0.185
K	0.000	0.000	0.000	0.001	0.125	0.000	0.001	0.000	0.267	1.711	0.000	0.000	1.827	0.005	0.000	0.002	0.279	0.005
X_{Mg}	0.78	0.61	0.81	0.87	0.78	0.69	0.43	0.77	0.73	0.82	0.77	0.84	0.88		0.82	0.91	0.91	

respectively.

5.3. Recrystallization conditions

We cannot estimate the pressure conditions for the ultramafic to mafic granulites by applying garnet-bearing mineral pair geobarometers because the rocks contain no garnet (Ren et al., 1992). Therefore, only two-pyroxene thermometers can be applied to estimate their recrystallization temperature; the estimated results are listed in Table 3. A recrystallized metamorphic temperature of 850 °C has been obtained from a mafic granulite in this region (Ren et al., 1992), which may be regarded as the reference temperature of peak granulite metamorphism.

Relatively low temperature estimates were obtained for three samples from the thermometer of Wells (1977), while relatively high estimates of 860–900 °C were calculated with the thermometer of Wood and Banno (1973) (Table 3). Considering that the higher estimates are consistent with the peak metamorphic temperatures of granulite facies metamorphism in the region (Tong et al., 2014), the relatively high estimates of 860–900 °C may be inferred to reflect the real peak recrystallization temperatures for the ultramafic rocks during granulite facies metamorphism.

6. Geochemistry

6.1. Major and trace elements

Major and trace element compositions of the ultramafic and mafic granulites are listed in Table 4. Whole rock SiO_2 contents range from 43.1 to 44.2 wt% for dark ultramafic granulites, 52.4 to 54.9 wt% for greenish ultramafic granulites, and 45.7 to 49.1 wt% for mafic granulites, with one exception (up to 60.4 wt%) for sample 7012 (Table 4), likely due to high modal contents of plagioclase and quartz in the latter. In addition, ultramafic granulites show high MgO contents from 19.4 to 22.9 wt%, while mafic granulites display relatively high Al_2O_3 contents from 10.9 to 20.0 wt%. Their $Mg^#$ values are also high and range from

0.71 to 0.73 for dark ultramafic granulite, from 0.82 to 0.84 for greenish ultramafic granulite and from 0.73 to 0.78 for mafic granulite, by comparison with the lower $Mg^#$ values (0.46–0.59) for mafic granulite reported by Wang et al. (1994) (Table 4). On the Al_2O_3-CaO-MgO diagram of Coleman (1977), all the dark and greenish ultramafic granulites plot in the field of ultramafic cumulates, while all the mafic granulites plot in the field of mafic cumulates (Fig. 4). Thus, the bulk rock compositions suggest that their precursors are ultramafic and mafic cumulates, respectively.

The ultramafic granulites have high bulk rock Cr and Ni contents: [Cr] up to 1826 ppm for dark ultramafic granulite and 1813 ppm for greenish ultramafic granulite, and [Ni] up to 1400 ppm for dark ultramafic granulite and 1035 ppm for greenish ultramafic granulite (Table 4). Except for one sample with a high Cr content (up to 1460 ppm), the other mafic granulites have low Cr and Ni contents likely related to fractional crystallization of their initial magmas. The Ti/Zr ratios of 110 and 112 for ultramafic granulite samples 92335 and 92322, respectively, are consistent with the Ti/Zr ratio reported for one mafic granulite sample by Wang et al. (1994) (Table 4), and are identical to that (110) in chondrite (Sun and Nesbitt, 1977), suggesting a source in the upper mantle. Geochemical diagrams (Fig. 5) show that the contents of major and trace elements vary versus *mg* values as a rough index of magmatic differentiation (Jahn et al., 1999). The overall variations in major elements are consistent with the *mg* variation.

On the primitive mantle (PM) normalized spider diagrams (Fig. 6), nearly all the ultramafic granulites show distinctive negative anomalies of Nb, Sr and Ti, and positive anomalies of Rb; one sample is enriched in K (Fig. 6a). For the mafic granulites, sample 9285a shows very obvious negative anomalies of Nb, P and Ti, sample 9285b has positive Rb and K anomalies, while samples 9285b and 7012 show negative Sr and Ti anomalies (Fig. 6b). The pronounced negative Nb anomalies in the granulite samples imply a subduction-related tectonic setting for the origin of their precursors (Munksgaard et al., 1992; Zhao et al., 1997), while low TiO_2 values, relative Nb depletion and some K-enrichment in the ultramafic and mafic granulites also indicate their derivation from arc basalts (Jahn, 1990; Munksgaard et al., 1992).
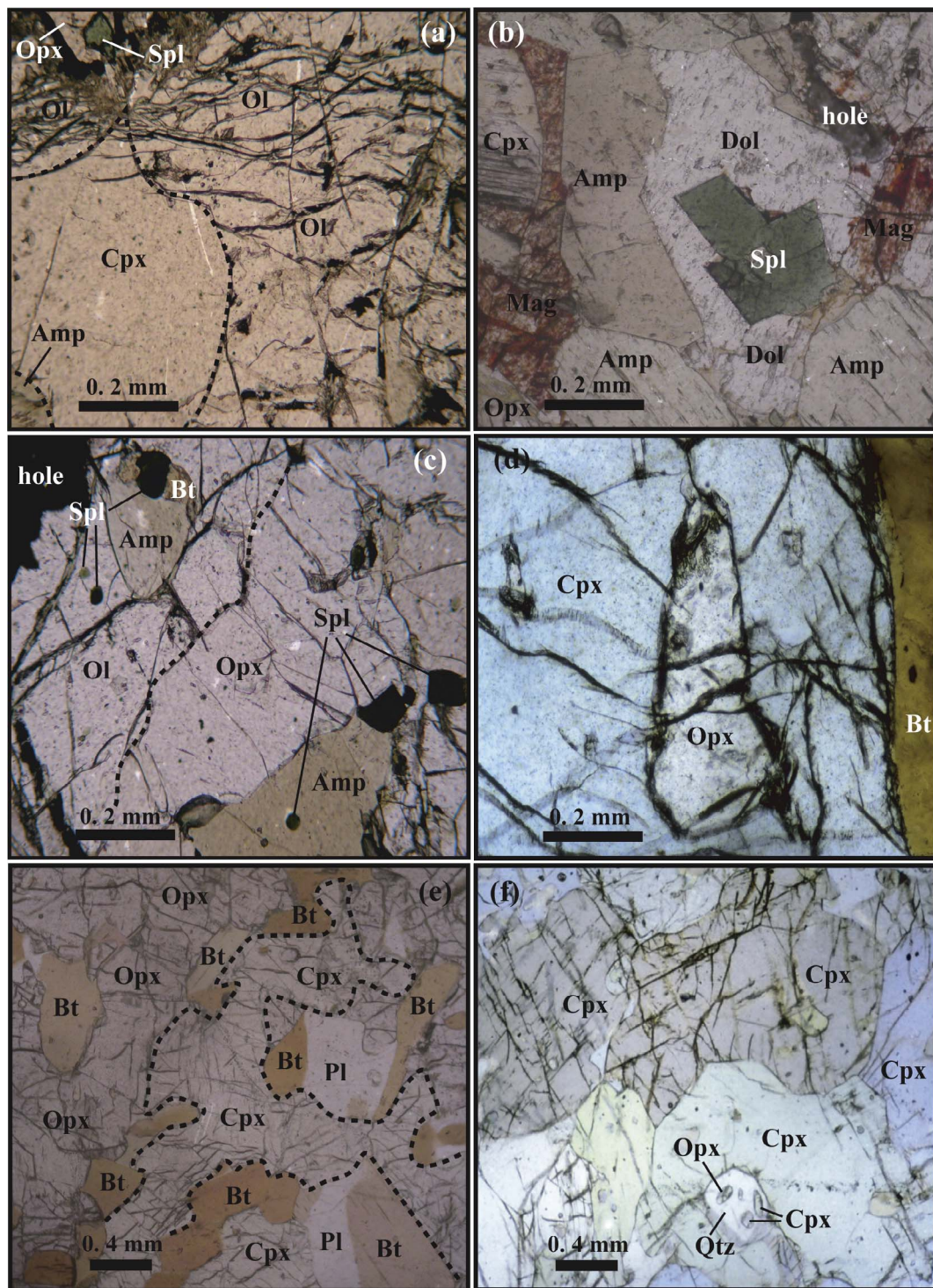
Fig. 3. Representative photomicrographs showing textural relations of ultramafic granulites from the Larsemann Hills. (a) Deformed olivine grains, sample 9204, Stornes Peninsula; (b) Magnesite growth on clinopyroxene grain, and spinel grain surrounded by dolomite, sample 9204, Stornes Peninsula; (c) Spinel-amphibole-biotite inclusions in an olivine grain, sample 92335, Stornes Penisula; (d) an orthopyroxene inclusion in a clinopyroxene grain, sample 9267, Striped Island; (e) biotite inclusions in an orthopyroxene grain, sample 9267, Striped Island; (f) small orthopyroxene and clinopyroxene grains together with quartz occur as inclusions in a large clinopyroxene grain, sample 92322, Steinnes Peninsula. Mineral abbreviations see Table 1.

6.2. REE

The rare earth element (REE) data for the ultramafic and mafic granulites are presented in Table 5. Chondrite-normalized REE patterns are shown in Fig. 7. For the ultramafic granulites, the total REE contents are low and range from 16.3 to 75.9 ppm, with $(La/Yb)_N = 3.2–7.0$ and $(La/Sm)_N = 1.4–3.1$ (Table 5). Their REE patterns show slight

enrichment in LREE, with no apparent Eu anomalies ($\delta Eu = 0.81–1.03$) (Fig. 7a). For the mafic granulites, the total REE contents are higher than those of the ultramafic granulites, and range from 43.6 to 158.6, with $(La/Yb)_N = 2.3–8.0$ and $(La/Sm)_N = 1.3–3.7$ (Table 5). The REE pattern for sample 7012 is a relatively flat with a small negative Eu anomaly ($\delta Eu = 0.75$), whereas the REE patterns in the other two samples show pronounced differentiation of the LREE and HREE, with

Table 3
Estimates of equilibrium temperature based on Opx-Cpx thermometers for representative ultramafic granulites (samples 9204, 9267 and 92322). Abbreviations: WB, Wood and Banno (1973), W, Wells (1977).

	9204 T (°C)	9267 T (°C)	92322 T (°C)
WB	867	859	902
W	796	813	836

an apparent negative Eu anomaly (δEu = 0.60) and a positive Eu anomaly (δEu = 1.55), respectively (Fig. 7a). As the two mafic granulites occur as interlayered bodies in field, these chemical features may be ascribed to element fractionation during crystallization.

7. Discussion

7.1. Ages of protoliths and metamorphism

Available geochronological data on mafic granulites and orthogneisses from the Larsemann Hills region show that their protoliths were formed in the late Mesoproterozoic at ~1100 Ma and then experienced

Fig. 4. An Al_2O_3-CaO-MgO diagram (in wt%) (fields after Coleman, 1977) for ultramafic granulite pods and lenses, and mafic granulite boudins from the Larsemann Hills (black circles); squares are the ultramafic granulite boudins from the Bolingen Islands (after Thost et al., 1992), open circles are after Wang et al. (1994), and cross is after Tong et al. (1995).

a major granulite facies metamorphism in the early Neoproterozic at 990–900 Ma; the isotopic systematics were afterwards variably reset by the early Palaeozoic Pan-African thermal event at ~530 Ma (Table 6).

Table 4
Bulk-rock major and trace element concentrations of the ultramafic and mafic granulites from the Larsemann Hills.

	Ultramafic granulite					Mafic granulite			Mafic granulite*		
	9204	92335	7035	9267	92322	9285a	9285b	7012	212(30)	212(35)	208(02)
Major elements (in wt%)											
SiO_2	43.06	42.41	44.19	52.37	54.93	49.09	48.92	60.43	45.71	46.66	48.64
TiO_2	1.43	1.05	1.45	0.53	0.09	0.32	0.87	1.63	3.86	2.34	0.94
Al_2O_3	8.32	7.42	7.02	5.42	3.66	20.03	11.11	10.93	13.30	13.63	15.28
Fe_2O_3	5.00	2.25	4.52	0.61	0.39	0.40	0.59	5.84	1.77	1.98	1.67
CaO	6.53	4.44	6.61	6.44	11.96	12.69	8.41	5.79	10.05	11.28	12.01
MgO	21.18	22.85	20.30	21.56	19.40	7.91	17.18	1.14	6.52	7.45	7.22
FeO	10.71	16.18	11.20	9.00	7.03	5.49	9.52	10.24	13.33	11.14	8.27
MnO	0.27	0.36	0.29	0.25	0.24	0.19	0.21	0.29	0.23	0.19	0.17
Na_2O	0.60	0.67	0.77	0.24	0.47	1.85	0.15	1.34	2.33	2.41	2.72
K_2O	0.38	0.52	0.18	2.39	0.22	0.31	1.80	0.20	0.40	0.64	0.58
P_2O_5	0.14	0.18	0.12	0.10	0.01	0.01	0.13	0.51	0.49	0.26	0.07
$H_2O +$	0.00	1.13	1.45	0.92	0.89	0.88	0.88	0.79	0.80	0.42	0.80
LOI	1.39	0.98	1.55	0.45	0.84	0.55	0.16	1.03	1.16	1.20	1.01
Totals	99.01	100.44	99.65	100.35	100.13	99.72	99.93	100.16	99.98	99.66	99.48
Trace elements (in ppm)											
Zr	70	90	88	24	4	33	92	231	244	144	51
Y	22	35	48	34	10	20	30	45	43	44	19
Sr	79	48	58	11	10	336	59	137	153	140	166
Rb	81	26	37	132	8	12	93	6	5	6	6
Ga	23	13	7	10	10	19	5	12	28	21	17
Zn	169	280	215	201	136	89	184	175	139	123	113
Ni	806	672	1400	1035	821	110	469	40	64	56	90
Co	72	58	45	4	31	55	12	31	n.a.	n.a.	n.a.
Cr	1332	1826	1231	1157	1813	580	1460	191	102	251	528
V	0	153	238	83	13	41	114	103	526	393	290
Ti	5227	9859	8444	2998	449	2059	5141	10,149	23,232	14,064	5664
La	23	24	27	6	15	8	12	30	n.a.	n.a.	n.a.
Ce	23	25	18	13	8	16	30	42	n.a.	n.a.	n.a.
Ba	202	126	54	201	46	76	184	16	67	79	44
Sc	24	21	24	24	24	33	29	28	n.a.	n.a.	n.a.
Nb	3	6	7	3	2	1	9	11	29	19	5
Pb	5	6	3	2	4	9	7	6	18	22	28
Th	2	2.3	1.3	2.6	2.1	0.9	0.8	0.2	n.a.	n.a.	n.a.
U	1	0.4	0.5	0.7	1.2	0.3	0.3	0.1	n.a.	n.a.	n.a.
Mg#	0.73	0.71	0.71	0.82	0.84	0.73	0.78	0.12	0.46	0.53	0.59
Ti/Zr	75	110	96	125	112	62	56	44	95	98	110
K/Rb	39	166	40	150	228	214	161	277	664	885	802
Rb/Sr	1.03	0.54	0.64	12.00	0.80	0.04	1.58	0.04	0.03	0.04	0.04
Sr/Ba	0.39	0.38	1.07	0.05	0.22	4.42	0.32	8.56	2.28	1.77	3.77
La/Nb	7.7	4.0	3.9	2.0	7.5	8.0	1.3	2.7	n.	n.	n.

Notice: The data of mafic granulites* are from Wang et al. (1994). Mg# value represents the molecular proportion of MgO/(MgO + FeO), assuming 90% of total iron as ferrous iron. (Note: the sentences should be below the table.)
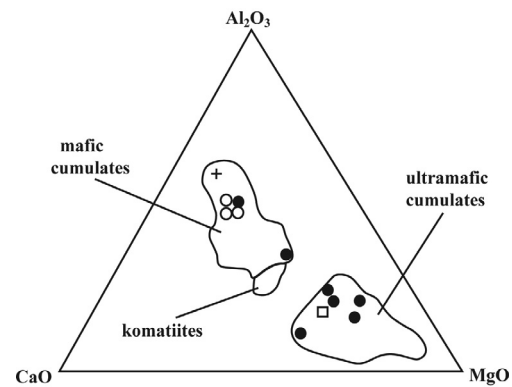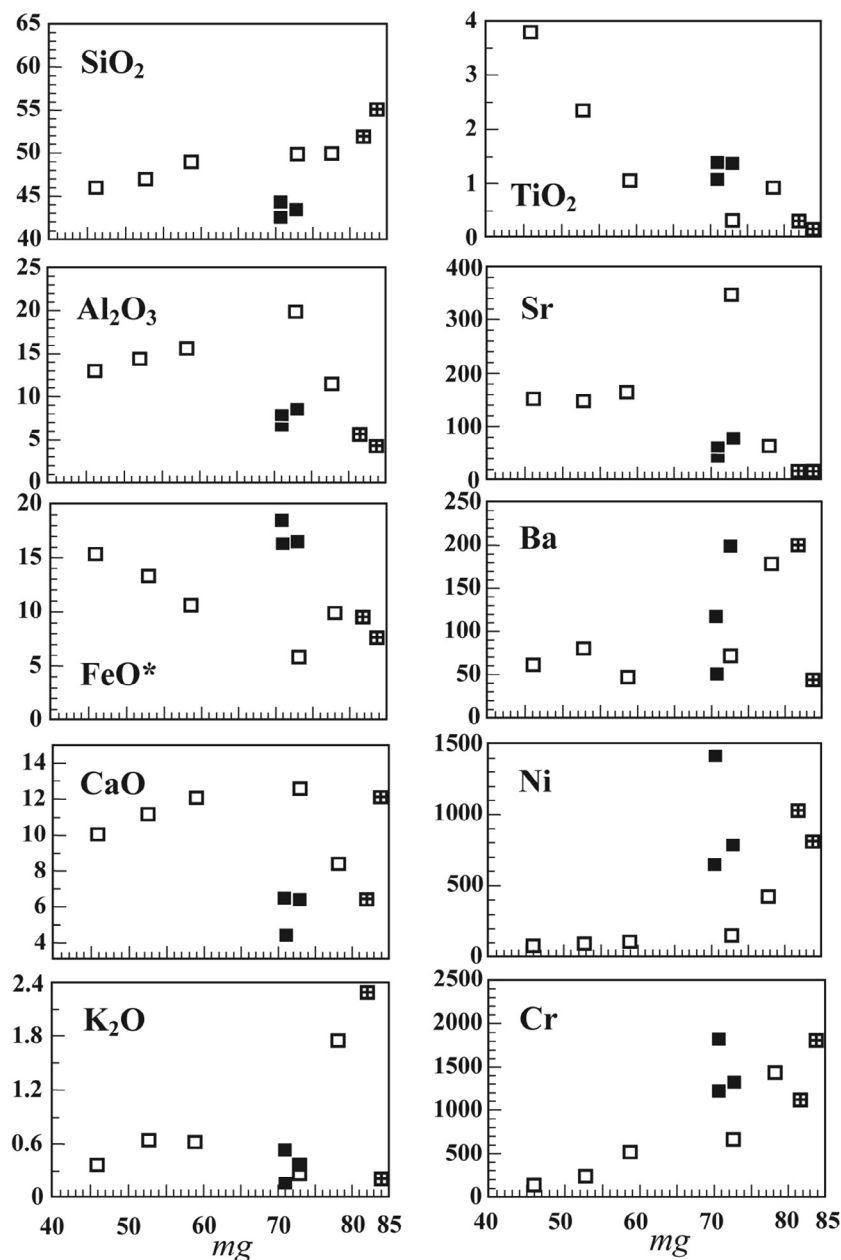
Fig. 5. Co-variation diagrams for major and trace elements as a function of *mg* value, which represents the molecular proportions of $100 \times MgO/(MgO + FeO)$, assuming 90% of total iron as ferrous iron (after Jahn et al., 1999). Black and cross boxes are ultramafic granulite, and blank box is mafic granulite.

SHRIMP zircon U-Pb dating for the region, yields the following protolith ages: 1126 ± 20 Ma for a mafic granulite, 1133 ± 12, 1119 ± 13 Ma and 1126 ± 11 Ma for three felsic orthogneisses (Wang et al., 2008), and 1124 ± 24 Ma for one felsic orthogneiss (Grew et al., 2012). Likewise, early Neoproterozoic metamorphic zircon U-Pb ages were also reported from the region: 987 ± 7 Ma, ~990–940 Ma and ~950–900 Ma for three mafic granulites, 981 ± 13 Ma and 997 ± 13 Ma for two felsic orthogneisses, 970 ± 16 Ma and 937 ± 21 Ma for two paragneisses (Wang et al., 2008), and 991 ± 12 Ma for one felsic orthogneiss (Grew et al., 2012). Furthermore, whole rock Pb isotope compositions for four ultramafic granulite samples in the region defined an isochron with an age of 950 ± 180 Ma, which was interpreted to date early Neoproterozoic metamorphism of the ultramafic granulite, albeit with a large uncertainty (Chen et al., 1998). A cooling Ar-Ar plateau age of 1059 ± 3 Ma obtained from orthopyroxene in a structurally early mafic granulite within the host paragneiss in the region (Tong et al., 2002), indicates that the protolith age of mafic granulite should be older than ~1060 Ma. Additionally, deformed ultramafic granulite

occurs in the host paragneiss (Fig. 2b). Therefore, the Ar-Ar age and deformation imply that ultramafic and mafic granulites in the paragneiss were tectonically inserted after deposition of the precursors to the cover paragneiss. The Rb-Sr isotope data indicate a resetting of the system during the Pan-African thermal event (Chen et al., 1998). In addition, metamorphic zircon giving early Palaeozoic U-Pb ages is also evidence for the Pan-African thermal overprint on the felsic orthogneisses and paragneisses in the region (Wang et al., 2008; Grew et al., 2012) (Table 6). Similar protolith ages as well as early Neoproterozoic and early Palaeozoic metamorphic ages were also reported for mafic granulites and felsic orthogneisses in the southwestern Prydz Bay and areas east of the Amery Ice Shelf (Liu et al., 2009, 2014) (Table 6).

7.2. Tectonic implications

Ultramafic and mafic granulites occur as pods or lenses, boudins or layered bodies in the paragneisses and orthogneisses in the Larsemann Hills region and adjacent areas. The ultramafic spinel-olivine and two-pyroxene granulites are probably derived from lherzolite and
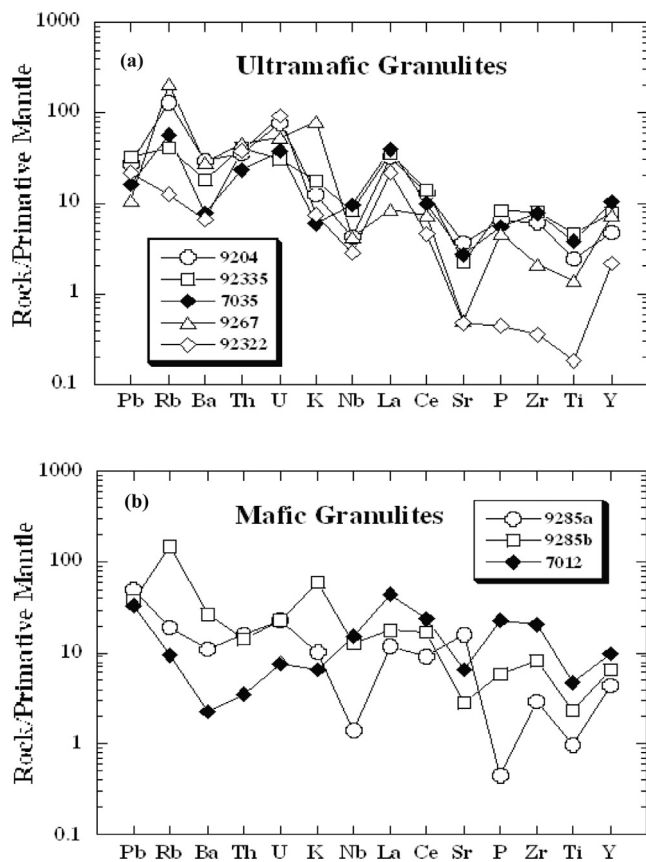
Fig. 6. Primitive-mantle (PM) normalized spider diagrams for ultramafic granulites (a) and mafic granulites (b) from the Larsemann Hills. PM values are from Sun and McDonough (1989).

Fig. 7. Chondrite-normalized REE distribution patterns for ultramafic granulites (a) and mafic granulites (b) from the Larsemann Hills. Chondrite values are from Masuda et al. (1973) divided by 1.2.

Table 5
Rare earth element (REE) analyses (in parts per million) for the ultramafic and mafic granulites from the Larsemann Hills. Notice: δEu = Eu/Eu*, Eu* = (Sm × Gd)$^{1/2}$.

	Ultramafic granulite					Mafic granulite		
	9204	92335	7035	9267	92322	9285a	9285b	7012
La	9.18	12.49	7.30	6.35	3.03	9.32	12.03	17.87
Ce	24.81	26.79	17.88	15.36	6.82	18.85	33.16	45.51
Pr	3.05	3.44	2.55	2.05	0.78	2.18	4.50	6.63
Nd	14.23	14.63	11.91	8.86	2.91	7.98	19.54	31.61
Sm	3.58	3.50	3.24	2.02	0.60	1.56	4.60	8.64
Eu	1.29	1.04	0.97	0.54	0.25	0.82	0.87	2.24
Gd	4.12	3.99	3.41	2.08	0.62	1.73	4.45	9.91
Tb	0.76	0.64	0.56	0.30	0.09	0.25	0.65	1.64
Dy	4.33	3.70	3.13	1.70	0.50	1.43	3.48	9.83
Ho	0.83	0.79	0.60	0.34	0.10	0.28	0.64	2.04
Er	2.03	2.27	1.63	0.99	0.28	0.84	1.75	5.80
Tm	0.32	0.32	0.22	0.14	0.04	0.21	0.24	0.81
Yb	1.87	1.95	1.32	0.88	0.28	0.77	1.43	5.24
Lu	0.28	0.30	0.19	0.14	0.04	0.12	0.21	0.80
ΣREE	70.68	75.85	54.91	41.75	16.34	46.34	87.55	158.57
LREE/HREE	3.86	4.43	3.96	5.35	7.38	10.88	9.42	5.06
δEu	1.03	0.85	0.89	0.89	0.81	1.55	0.60	0.75
(La/Yb)$_N$	3.24	4.23	3.65	4.77	7.02	8.00	5.55	2.25
(La/Sm)$_N$	1.57	2.19	1.38	1.93	3.09	3.68	1.60	1.27
(Gd/Yb)$_N$	1.77	1.64	2.07	1.90	1.74	1.81	2.50	1.52

pyroxenite, respectively, while the mafic two-pyroxene-plagioclase granulites are likely metamorphosed gabbros. P-T estimates show that they recrystallized at 860–900 °C in line with granulite facies metamorphism. These results are consistent with the peak metamorphic temperatures of 870 °C and 900 °C for the metamorphic rocks reported by Tong and Liu (1997) and Tong et al. (2014), and also roughly
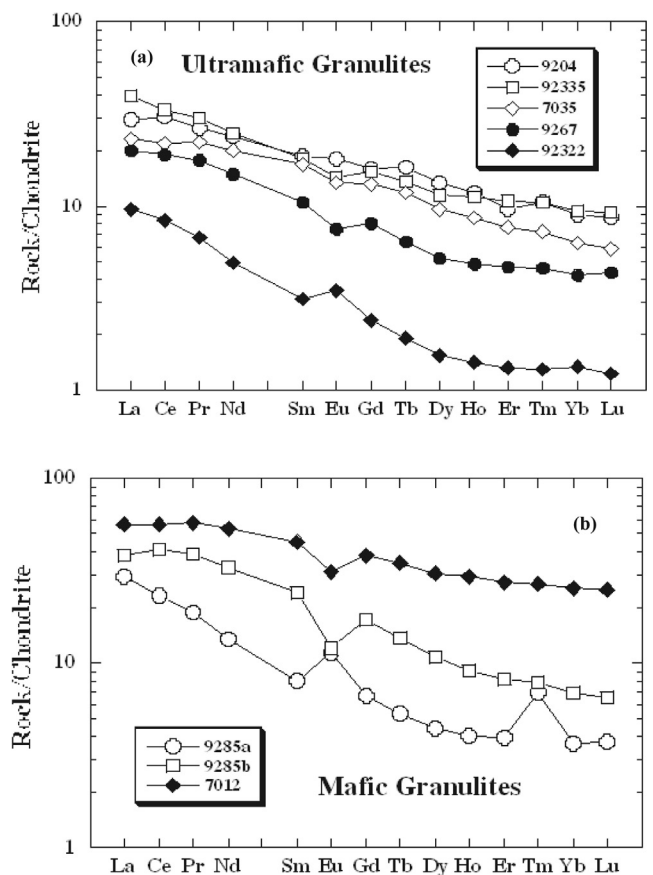
consistent with the peak metamorphic temperature of 850 °C for the mafic granulites in the region (Ren et al., 1992). The available isotope chronological data support assignment of an early Neoproterozoic (990–900 Ma) age to the peak granulite facies metamorphism of ultramafic and mafic granulites in the Larsemann Hills region (Chen et al., 1998; Wang et al., 2008; Grew et al., 2012), rather than the early Palaeozoic (Pan-African) at 550–500 Ma as previously thought (Ren et al., 1992; Hensen and Zhou, 1995; Zhao et al., 1995; Carson et al., 1996, 1997; Fitzsimons et al., 1997).

Whole rock major and trace element compositions including relatively high Mg$^{\#}$ values of ultramafic to mafic granulites are consistent with their derivation from igneous mafic and ultramafic cumulates (Table 4, Fig. 4). Their trace element patterns show pronounced negative Nb and Ti anomalies (Fig. 6) suggesting a subduction-related tectonic setting for the origin of their precursors (Munksgaard et al., 1992; Zhao et al., 1997), while low TiO$_2$ values, relative Nb depletion and K-enrichment also indicate their derivation from arc basalts (Jahn, 1990; Munksgaard et al., 1992). Therefore, the ultramafic and mafic granulites in the region may have been initially generated in a subduction zone environment related to arc setting. Similar conclusions were also inferred for the early Neoproterozoic mafic granulites in the northern Prince Charles Mountains (nPCMs) (Munksgaard et al., 1992; Zhao et al., 1997).

The ultramafic and mafic granulites in the region may have been formed in a continental arc setting as well because negative Nb anomalies are also characteristic of typical continental crust (Jahn et al., 1999), this implies that. This suggestion is consistent with the inference that the precursors of boron-bearing mineral assemblages in the paragneiss in the region originated in a back-arc basin inboard of an active continental arc (Grew et al., 2012, 2013). SHRIMP zircon U-Pb

Table 6
Summary of Ar-Ar, Pb-Pb and U-Pb age data of metamorphic rocks from the Larsemann Hills and southwestern Prydz Bay.

Location	Rock type	Method	Protolith Age (Ma)	Cooling Age (Ma)	Metamorphic Age (Ma)	Reference
Larsemann Hills	Amphibolite	Ar-Ar		1036 ± 14		Tong et al. (1998)
	Mafic granulite	Ar-Ar		1059 ± 3		Tong et al. (2002)
	Ultramafic granulite	Pb-Pb			950 ± 180	Chen et al. (1998)
	Mafic granulite	SHRIMP			~990–940	Wang et al. (2008)
	Mafic granulite	SHRIMP			978 ± 7	Wang et al. (2008)
	Mafic granulite	SHRIMP			~950–900	Wang et al. (2008)
	Felsic orthogneiss	SHRIMP	1126 ± 11		1031 ± 29	Wang et al. (2008)
	Felsic orthogneiss	SHRIMP	1124 ± 24		991 ± 12, 530 ± 3	Grew et al. (2012)
	Paragneiss	SHRIMP			970 ± 16	Wang et al. (2008)
	Paragneiss	SHRIMP			937 ± 21, 539 ± 11	Wang et al. (2008)
Steinnes Peninsula	Mafic granulite	SHRIMP			1007 ± 10	Wang et al. (2008)
	Felsic orthogneiss	SHRIMP	1133 ± 12		981 ± 13, 529 ± 8	Wang et al. (2008)
	Felsic orthogneiss	SHRIMP	1119 ± 13		997 ± 13, 546 ± 7	Wang et al. (2008)
Søstrene Island	Mafic granulite	SHRIMP			~1000–530	Liu et al. (2009)
	Felsic orthogneiss	SHRIMP	1119 ± 13		922 ± 10	Liu et al. (2014)
Manning Nunataks	Felsic orthogneiss	SHRIMP	1347 ± 22		968 ± 97, 529 ± 4	Liu et al. (2014)
Mistichelli Hills	Felsic orthogneiss	SHRIMP	1179 ± 23		968 ± 19, 536 ± 11	Liu et al. (2009)
McKaskle Hills	Mafic granulite	SHRIMP	1137 ± 46			Liu et al. (2007)
	Felsic orthogneiss	SHRIMP	1174 ± 26		529 ± 11	Liu et al. (2007)
Reinbolt Hills	Mafic granulite	SHRIMP			927 ± 29	Liu et al. (2009)
	Felsic orthogneiss	SHRIMP	1042 ± 24		925 ± 13, 900 ± 14	Liu et al. (2009)

ages for mafic granulites and felsic orthogneisses and paragneisses indicate that the paragneiss precursors in the region formed ~1000 Ma ago, further suggesting that these rocks experienced first granulite facies metamorphic event in the early Neoproterozoic (990–900 Ma), and subsequently were affected by the early Palaeozoic Pan-African metamorphic event at ~530 Ma (Wang et al., 2008; Grew et al., 2012). Thus, the chronological data and early Neoproterozoic metamorphic evolutionary history suggest broad similarities between the Larsemann Hills and nPCMs. It appears that both the Larsemann Hills and nPCMs represent important parts of the Rayner Complex, hence both of them likely belonged to the large-scale Rayner orogen (Grew et al., 2012; Tong et al., 2014). Therefore, this study suggests that ultramafic to mafic granulites were formed simultaneously with the regional peak granulite facies metamorphism in the Larsemann Hills region in a subduction-related continental back-arc basin environment associated with an arc-continent collision during the early Neoproterozoic (990–900 Ma) Rayner orogeny.

Recent regional geochronological and geochemical studies also show that the mafic granulites and felsic orthogneisses from the southwestern Prydz Bay region and the eastern Amery Ice Shelf represent an eastern extension of the Rayner Complex, which constitutes a large single continental arc (Liu et al., 2014). It has been suggested that these rocks formed as a result of arc-continent collision during the early Neoproterozoic (>970 Ma) Rayner orogeny (Liu et al., 2014), well consistent with the inferences of this study for the Larsemann Hills region. However, the scenario of an arc-continent collision subsequently followed by a continent-continent collision at 940–900 Ma in the Prydz Belt implies a two-stage orogeny, whereas Grew et al. (2012) concluded that data from the Larsemann Hills did not support the existence of two distinct magmatic episodes in the Rayner orogeny. Thus, this point needs to be clarified and more dating should be done for the region in future.

8. Conclusions

Mafic and ultramafic granulites occur as lenses or boudins in the late Proterozioc (~1000 Ma) paragneiss and felsic orthogneiss in the Larsemann Hills, East Antarctica. The ultramafic and mafic granulites have spinel-olivine-bearing and two-pyroxene-bearing mineral assemblages, and show compositional features of igneous cumulate, which recrystallized at 860–900 °C.

The high whole rock $Mg^{\#}$ values and high Cr and Ni contents of the ultramafic granulites are consistent with the derivation from igneous cumulates. Relatively low contents of Cr (191–580 ppm) and Ni (40–110 ppm) in mafic granulites may be attributed to fractional crystallization of their parental magmas. Pronounced negative Nb anomalies relate them to subduction-related magmas, while low TiO_2 values and K-enrichment in mafic granulites indicate links to arc basalts.

Thus, the ultramafic to mafic granulites in the Larsemann Hills region may have been formed concurrently with regional peak granulite facies metamorphism in a subduction-related continental back-arc basin environment associated with an arc-continent collision during the early Neoproterozoic (990–900 Ma) Rayner orogeny.

References

Black, L.P., Kinny, P.D., Sheraton, J.W., Delor, C.P., 1991. Rapid production and evolution of the late Archaean felsic crust in the Vestfold Block of East Antarctica. Precam. Res. 50, 283–310.

Carson, C.J., Grew, E.S., 2007. Geology of the Larsemann Hills region, Antarctica, First ed., 1:25,000 Scale Map, Canberra, Geoscience Australia.

Carson, C.J., Dirks, P.H.G.M., Hand, M., Sims, J.P., Wilson, C.J.L., 1995a. Compressional and extensional tectonics in low-medium pressure granulites from the Larsemann

Hills, East Antarctica. Geol. Mag. 132, 151–170.

Carson, C.J., Hand, M., Dirks, P.H.G.M., 1995b. Stable coexistence of grandidierite and kornerupine during medium pressure granulite facies metamorphism. Mineral. Mag. 59, 327–339.

Carson, C.J., Fanning, C.M., Wilson, C.J.L., 1996. Timing of the Progress Granite, Larsemann Hills: evidence for Early Palaeozoic orogenesis within the east Antarctic Shield and implications for Gondwana assembly. Aust. J. Earth Sci. 43, 539–553.

Carson, C.J., Powell, R., Wilson, C.J.L., Dirks, P.H.G.M., 1997. Partial melting during tectonic exhumation of a granulite terrane: an example from the Larsemann Hills, East Antarctica. J. Metamorphic Geol. 19, 105–126.

Chen, F., Tong, L., Liu, X., 1998. Nd, Sr, and Pb isotope systematics of ultramafic rocks from the Larsemann Hills, East Antarctica. Chin. Sci. Bull. 43 (1) 20–20.

Coleman, R.G., 1977. Ophiolites. Springer Verlag, New York 229p.

Dirks, P.H.G.M., Hand, M., 1995. Clarifying temperature-pressure paths via structures in granulite from the Bolingen Islands, Antarctica. Aust. J. Earth Sci. 42, 157–172.

Dirks, P.H.G.M., Wilson, C.J.L., 1995. Crustal evolution of the east Antarctic mobile belt in Prydz Bay: continental collision at 500 Ma? Precam. Res. 75, 189–207.

Dirks, P.H.G.M., Carson, C.J., Wilson, C.J.L., 1993. The deformation history of the Larsemann Hills, Prydz Bay: the importance of the Pan-African (500 Ma) in East Antarctica. Antarctic Sci. 5, 179–192.

Fitzsimons, I.C.W., 1996. Metapelitic migmatites from Brattstrand Bluffs, east Antarctica-metamorphism, melting and exhumation of the mid-crust. J. Petrol. 37, 395–414.

Fitzsimons, I.C.W., 1997. The Brattstrand paragneiss and the Sostrene orthogneiss: a review of Pan-African metamorphism and Grenvilian relics in southern Prydz Bay. In: Ricci, C.A. (Ed.), The Antarctic Region: Geological Evolution and Processes. Terra Antartica Publ, Siena, pp. 121–130.

Fitzsimons, I.C.W., 2003. Proterozoic basement provinces of southern and southwestern Australia, and their correlation with Antarctica. In: Yoshida, M., et al. (Eds.), Proterozoic East Gondwana: Supercontinent Assembly and Breakup, vol. 206. Geol. Soc. Lond., Spec. Publ., pp. 93–130.

Fitzsimons, I.C.W., Harley, S.L., 1991. Geological relationships in high-grade gneiss of the Brattstrand Bluffs coastline, Prydz Bay, east Antarctica. Aust. J. Earth Sci. 38, 497–519.

Fitzsimons, I.C.W., Kinny, P.D., Harley, S.L., 1997. Two stages of zircon and monazite growth in anatectic leucogneiss: SHRIMP constraints on the duration and intensity of Pan-African metamorphism in Prydz Bay, East Antarctica. Terra Nova 9, 47–51.

Grew, E.S., Armbruster, T., Medenbach, O., Yates, M.G., Carson, C.J., 2006. Stornesite-(Y), (Y, Ca)☐₂Na₆(Ca, Na)₈(Mg, Fe)₄₃(PO₄)₃₆, the first terrestrial Mg-dominant member of the fillowite group, from granulite-facies paragneiss in the Larsemann Hills, Prydz Bay, East Antarctica. Am. Mineral. 91, 1412–1424.

Grew, E.S., Armbruster, T., Medenbach, O., Yates, M.G., Carson, C.J., 2007. Chopinite, [(Mg, Fe)₃☐](PO₄)₂, a new mineral isostructural with sarcopside, from a fluorapatite segregation in granulite-facies paragneiss, Larsemann Hills, Prydz Bay, East Antarctica. Eur. J. Mineral. 19, 229–245.

Grew, E.S., Carson, C.J.L., Christy, A.G., Maas, R., Yaxley, G.M., Boger, S.D., Fanning, C.M., 2012. New constraints from U-Pb, Lu-Hf and Sm-Nd isotopic data on the timing of sedimentation and felsic magmatism in the Larsemann Hills, Prydz Bay, east Antarctica. Precam. Res. 206, 87–108.

Grew, E.S., Carson, C.J.L., Christy, A.G., Boger, S.D., 2013. Boron- and phosphate-rich rocks in the Larsemann Hills, Prydz Bay, East Antarctica: tectonic implications. In: Harley, S.L. et al., (Eds.), Antarctica and Supercontinent Evolution, vol. 383. Geol. Soc. Lond., Spec. Publ., pp. 73–94.

Harley, S.L., 1998. Ultrahigh temperature granulite metamorphism (1050 °C, 12 kbar) and decompression in garnet (Mg70)-orthopyroxene-sillimanite gneisses from the Rauer Islands, East Antarctica. J. Metamorphic Geol. 16, 541–562.

Harley, S.L., Snape, I., Fitzsimons, I.C.W., 1995. Regional correlations and terrane assembly in East Prydz Bay: evidence from the Rauer Group and Vestfold Hills. Terra Antart. 1, 49–60.

Hensen, B.J., Zhou, B., 1995. A Pan-African granulite facies metamorphic episode in Prydz Bay, Antarctica: evidence from Sm-Nd garnet dating. Aust. J. Earth Sci. 42, 249–258.

Hensen, B.J., Zhou, B., 1997. East Gondwana amalgamation by Pan-African collision? Evidence from Prydz Bay, east Antarctica. In: Ricci, C.A. (Ed.), The Antarctic Region: Geological Evolution and Processes. Terra Antartica Publ, Siena, pp. 115–119.

Hiroi, Y., Shiraishi, K., Motoyoshi, Y., 1991. Late Proterozoic paired metamorphic complex in East Antarctica, with special reference to the tectonic significance of ultramafic rocks. In: Thompson, M.R.A. (Ed.), Geological Evolution of Antarctica. Cambridge University Press, pp. 83–87.

Jahn, B.M., 1990. Origin of granulites: geochemical constraints from Archaean granulite facies rocks of the Sino-Korean Craton, China. In: Vielzeuf, D., Vidal, Ph. (Eds.), Granulites and Crustal Evolution. NATO ASI Series Kluwer Academic Publishers, Dordrecht, pp. 471–492.

Jahn, B.M., Wu, F., Lo, C.H., Tsai, C.H., 1999. Crustal-mantle interaction induced by deep subduction of the continental crust: geochemical and Sr-Nd isotopic evidence from post-collisional mafic-ultramafic intrusions of the northern Dabie complex, central China. Chem. Geol. 157, 119–146.

Kinny, P.D., Black, L.P., Sheraton, J.W., 1993. Zircon ages and the distribution of Archaean and Proterozoic rocks in the Rauer Islands. Antarct. Sci. 5, 193–206.

Lanyon, R., Black, L.P., Seitz, H.M., 1993. U-Pb zircon dating of mafic dykes and its application to the Proterozoic geological history of the Vestfold Hills, East Antarctica. Contrib. Mineral. Petrol. 115, 184–203.

Li, X.H., Li, Z.X., Wingate, M.T.D., Chung, S.L., Liu, Y., Lin, G.C., Li, W.X., 2006. Geochemistry of the 755 Ma Mundine Well dyke swarm, northwestern Australia: part of a Neoproterozoic mantle superplume beneath Rodinia? Precam. Res. 146, 1–15.

Liu, X., Zhao, Y., Zhao, G.C., Jian, P., Xu, G., 2007. Petrology and geochronology of granulites from the McKaskle Hills, eastern Amery Ice Shelf, Antarctica, and

implications for the evolution of the Prydz Belt. J. Petrol. 48, 1443–1470.

Liu, X., Zhao, Y., Song, B., Liu, J., Cui, J., 2009. SHRIMP U-Pb zircon geochronology of high-grade rocks and charnockites from the eastern Amery Ice Shelf and south-western Prydz Bay, East Antarctica: constraints on Late Mesoproterozoic to Cambrian tectonothermal events related to supercontinent assembly. Gondwana Res. 16, 342–361.

Liu, X., Zhao, Y., Hu, J., 2013. The c.1000–900 Ma and c.550–500 Ma tectonthermal events in the Prince Charles Mountains-Prydz Bay region, East Antarctica, and their relations to supercontinent evolution. In: Harley, S.L., et al., (Eds.), Antarctica and Supercontinent Evolution, vol. 383. Geol. Soc. Lond., Spec. Publ., pp. 95–112.

Liu, X., Wang, W., Zhao, Y., Liu, J., Song, B., 2014a. Early Neoproterozoic granulite facies metamorphism of mafic dykes from the Vestfold Block, East Antarctica. J. Metamorphic Geol. 32, 1041–1062.

Liu, X., Jahn, B.M., Zhao, Y., Liu, J., Ren, L., 2014b. Geochemistry and geochronology of Mesoproterozoic basement rocks from the eastern Amery Shelf and southwestern Prydz Bay, East Antarctica: implications for a long-lived magmatic accretion in a continental arc. Am. J. Sci. 314, 508–547.

MacGregor, J., Grew, E.S., De Hoog, J.C.M., Harley, S.L., Kowalski, P.M., Yates, M.G., Carson, C.J., 2013. Boron isotopic composition of tourmaline, prismatine, and grandidierite from granulite facies paragneisses in the Larsemann Hills, Prydz Bay, East Antarctica: evidence for a non-marine evaporate source. Geochim. Cosmochim. Acta 123, 261–283.

Masuda, A., Nakamura, N., Tanaka, T., 1973. Fine structures of mutually normalized rare-earth patterns of chondrites. Geochim. Cosmochim. Acta 37, 239–244.

Munksgaard, N.C., Thost, D.E., Hensen, B.J., 1992. Geochemistry of Proterozoic granulites from northern Prince Charles Mountains, East Antarctica. Antarct. Sci. 4, 59–69.

Pouchou, L., Pichoir, F., 1984. A new model for quantitative X-ray microanalysis. Res. Aerospat. 3, 167–192.

Ren, L., Zhao, Y., Liu, X., Chen, T., 1992. Re-examination of the metamorphic evolution of the Larsemann Hills, East Antarctica. In: Yoshida, Y. (Ed.), Recent Progress in Antarctic Earth Science. Terra Scientific Publishing, Tokyo, pp. 145–153.

Ren, L., Wang, Y., Zhao, Y., 2008. Sapphirine in the high-grade quartzofeldspathic gneiss of the Larsemann Hills, East Antarctica. Chin. J. Polar Sci. 19, 1–13.

Sheraton, J.W., Black, L.P., McCulloch, M.T., 1984. Regional geochemical and isotopic characteristics of high-grade metamorphics of the Prydz Bay area: the extent of Proterozoic reworking of Archaean continental crust in east Antarctica. Precam. Res. 26, 169–198.

Stüwe, K., Powell, R., 1989. Low pressure granulite facies metamorphism in the Larsemann Hills area, East Antarctica: petrology and tectonic implications for the Prydz Bay area. J. Metamorphic Geol. 7, 465–484.

Stüwe, K., Braun, H.M., Peer, H., 1989. Geology and structure of the Larsemann Hills area, East Antarctica. Aust. J. Earth Sci. 36, 219–241.

Sun, S.S., McDonough, W.F., 1989. Chemical and isotopic systematics of oceanic basalts: implications for mantle composition and processes. In: Saunders, A.D., Norry, M.J. (Eds.), Magmatism in the Ocean Basins, vol. 42. Geol. Soc. Lond., Spec. Publ., pp. 313–345.

Sun, S.S., Nesbitt, R.W., 1977. Chemical heterogeneity of the Archean mantle, composition of the earth and mantle evolution. Earth Planet. Sci. Lett. 35, 429–448.

Thost, D.E., Hensen, B.J., Motoyoshi, Y., 1991. Two-stage decompression in garnet-bearing mafic granulites from Sostrene Island, Prydz Bay, East Antarctica. J. Metamorphic Geol. 9, 245–256.

Thost, D.E., Motoyoshi, Y., Hensen, B.J., 1992. Mode of occurrence, geochemistry and mineral texture of ultramafic rocks from the Bolingen Islands, Prydz Bay, East Antarctica. In: Yoshida, Y. (Ed.), Recent Progress in Antarctic Earth Science. Terra Scientific Publ, Tokyo, pp. 113–118.

Tong, L., Liu, X., 1997. The prograde metamorphism of the Larsemann Hills, East Antarctica: evidence for an anticlockwise P-T path. In: Ricci, C.A. (Ed.), The Antarctic Region: Geological Evolution and Processes. Terra Antartica Publ, Siena, pp. 105–114.

Tong, L., Wilson, C.J.L., 2006. Tectonothermal evolution of the ultrahigh temperature metapelites from the Rauer Group, East Antarctica. Precam. Res. 149, 1–20.

Tong, L., Liu, X., Zhang, L., Chen, F., 1995. The U-Pb zircon chronology of mafic granulite from the Larsemann Hills, East Antarctica and its possible geological implications. Terra Antart. 2, 123–126.

Tong, L., Liu, X., Xu, P., Han, X., Zhao, Y., Ren, L., Wang, Y., 1997. Discovery of sapphirine-bearing hyperthene quartzite in the Larsemann Hills, East Antarctica and its geological significance. Chin. Sci. Bull. 42, 324–327.

Tong, L., Liu, X., Zhang, L., Chen, H., Chen, F., Wang, Y., Ren, L., 1998. The Ar-Ar ages of hornblendes in Grt-Pl-bearing amphibolite from the Larsemann Hills, East Antarctica and their geological implications. Chin. J. Polar Res. 9, 79–91 (English version).

Tong, L., Wilson, C.J.L., Liu, X., 2002. A high-grade event of ~1100 Ma preserved within the ~500 Ma mobile belt of the Larsemann Hills, East Antarctica: further evidence from Ar-Ar dating. Terra Antart. 9, 73–86.

Tong, L., Jahn, B.M., Chen, F., Liu, X., Wang, Y., 2006. Geochemistry of mafic to ultra-mafic granulites from the Larsemann Hills, East Antarctica. Geochim. Cosmochim. Acta 70 (18 (Supp.)), A654.

Tong, L., Liu, X., Wang, Y., Liang, X., 2014. Metamorphic P-T paths of metapelitic granulites from the Larsemann Hills, East Antarctica. Lithos 192–195, 102–115.

Wang, Y., Zhao, Y., Ren, L., Chen, T., Liu, X., Tong, L., 1994. Geochemical characteristics and medium pressure granulite facies metamorphism of mafic granulite rocks from the Larsemann Hills, East Antarctica. Antarct. Res. 6, 1–11 (in Chinese).

Wang, Y., Liu, D., Chung, S.L., Tong, L., Ren, L., 2008. SHRIMP zircon constraints from the Larsemann Hills region, Prydz Bay, for a late Mesoproterozoic to early Neoproterozoic tectono-thermal event in the East Antarctica. Am. J. Sci. 308, 573–617.

Wells, R.A., 1977. Pyroxene thermometry in simple and complex systems. Contr. Mineral.

Petrol. 62, 129–139.

Wilson, C.J.L., Quinn, C., Tong, L., Phillips, D., 2007. Early Palaeozoic intracratonic shears and post-tectonic cooling in the Rauer Group, Prydz Bay, East Antarctica constrained by $^{40}Ar/^{39}Ar$ thermochronology. Antarct. Sci. 19, 339–353.

Wood, B.J., Banno, S., 1973. Garnet-orthopyroxene and orthopyroxene-clinopyroxene relationship in simple and complex systems. Contr. Mineral. Petrol. 42, 109–124.

Zhang, L., Tong, L., Liu, X., Scharer, U., 1996. Conventional U-Pb ages of the high-grade metamorphic rocks in the Larsemann Hills, East Antarctica. In: Pang, Z. (Ed.), Advances in Solid Earth Sciences. Science Press, Beijing, pp. 27–35.

Zhao, J.X., Ellis, D.J., Kilpatrick, J.A., McCulloch, M.T., 1997. Geochemical and Sr-Nd isotopic studies of charnockites and related rocks in the northern Prince Charles Mountains, East Antarctica: implications for charnckite petrogenesis and Proterozoic crustal evolution. Precam. Res. 81, 37–66.

Zhao, Y., Liu, X., Song, B., Zhang, Z., Li, J., Yao, Y., Wang, Y., 1995. Constraints on the stratigraphic age of the Larsemann Hills, East Antarctica: possible implications for Neo-Proterzoic tectonics. Precam. Res. 75, 175–188.

Zhao, Y., Liu, X.H., Liu, X.C., Song, B., 2003. Pan-African events in Prydz Bay, East Antarctica, and their implications for East Gondwana tectonics. In: Yoshida, M., et al. (Eds.), Proterozoic East Gondwana: Supercontinent Assembly and Breakup, vol. 206. Geol. Soc. Lond., Spec. Publ., pp. 231–245.